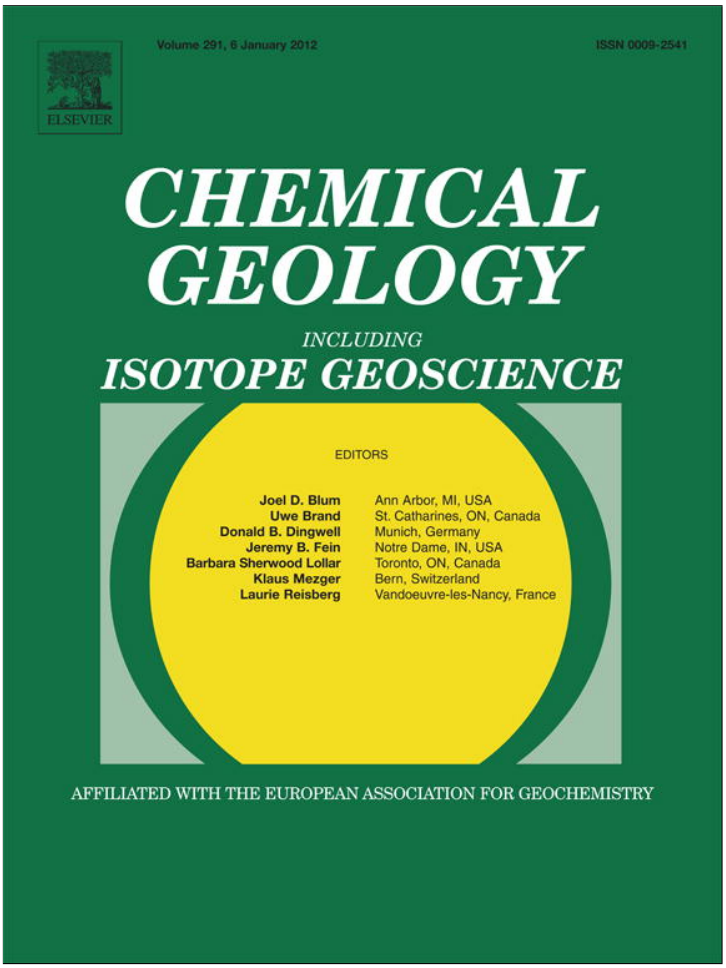

(This is a sample cover image for this issue. The actual cover is not yet available at this time.)

Chemical Geology 306-307 (2012) 129–138

Contents lists available at SciVerse ScienceDirect

Chemical Geology

journal homepage: www.elsevier.com/locate/chemgeo

Evolution from an anoxic to oxic deep ocean during the Ediacaran–Cambrian transition and implications for bioradiation

Jianguo Wang [a], Daizhao Chen [a,*], Detian Yan [b], Hengye Wei [a], Lei Xiang [a]

[a] Key Laboratory of Petroleum Resources Research, Institute of Geology and Geophysics, Chinese Academy of Sciences, Beijing 100029, China
[b] Key Laboratory of Tectonics and Petroleum Resources of Ministry of Education, University of Geosciences, Wuhan 430074, China

ARTICLE INFO

Article history:
Received 2 November 2011
Received in revised form 2 March 2012
Accepted 5 March 2012
Available online 13 March 2012

Editor: U. Brand

Keywords:
Ediacaran–Cambria transition
Carbon–sulfur cycling
Iron speciation
Oceanic anoxia and oxygenation
South China

ABSTRACT

The Ediacaran–Cambrian transition, one of the most critical intervals in Earth's history, is marked by dramatic biological, oceanic and geochemical turnovers. Here high-resolution carbon and sulfur isotopic data respectively for organic carbon and pyrite, and iron speciation data are presented from the deep-water Liuchapo and Niutitang Formations on the Yangtze block, South China. The carbon isotopic data, together with biostratigraphic and radiometric dating, offer the compelling evidence for the placement of Ediacaran–Cambrian boundary within the Liuchapo Formation (chert succession), and for its correlation with shallow-water equivalents elsewhere. In this context, iron speciation and sulfur isotopic data further suggest a predominant anoxic and ferruginous deep ocean over the transitional time until the middle Early Cambrian (Atdabanian or Stage 3) when the deep ocean was rapidly oxygenated. Coincidently, during this interval, large-body metazoans (i.e., sponges) abruptly appeared in the deep ocean, which was temporally associated with the highly diversified large-body skeletonized animals (i.e., Chengjiang Biota) which colonized in shallow-water niches particularly in southwestern China. This scenario suggests a causal link between deep oceanic oxygenation and the explosive diversification of large-body skeletonized organisms in the Early Cambrian.

1. Introduction

During the Ediacaran–Cambrian (E–C) transition, remarkable biological, oceanic and geochemical changes co-occurred simultaneously (e.g., Knoll and Carroll, 1999; Kimura and Watanabe, 2001; Amthor et al., 2003; Marshall, 2006); the most remarkable of these was the disappearance of Ediacaran fauna at the end of Neoproterozoic and subsequent explosive radiation of skeletonized animals from the Early Cambrian (Marshall, 2006). Animals, especially large animals, have a requirement of enough oxygen to sustain their life through aerobic metabolism (e.g., Graham et al., 1995; Knoll and Carroll, 1999; Marshall, 2006; Payne et al., 2009). Many studies suggested a rise in atmospheric oxygen concentration and subsequent oxygenation of ocean from the Ediacaran (Fike et al., 2006; Canfield et al., 2007); however, recent studies provided a different scenario and contended a view of an anoxic ocean, notably in the deep ocean in some areas (e.g., South China) during the E–C transition (Goldberg et al., 2007; Canfield et al. 2008; Chang et al., 2009).

At or near Earth's surface, the global carbon and sulfur cycles are intimately linked through biotic and abiotic processes, through which partitioning between the reduced (organic carbon, sulfide) and oxidized (carbonate, sulfate) reservoirs of carbon and sulfur is the primary control on atmospheric oxygen concentration (Berner, 1989). Perturbations in these cycles, such as enhanced burial of organic matter and pyrite or weathering, can be tracked by their isotopic compositions in sedimentary records (Gill et al., 2007). The iron (Fe) speciation has been extensively used in ancient fine-grained sediments to evaluate the redox conditions of the water column (e.g., Poulton et al., 2004; Canfield et al., 2008; Shen et al., 2008). Previous studies showed that the oceanic anoxic state can be further specified by Fe speciation data as either euxinic or ferruginous (e.g., Poulton et al., 2004; Canfield et al., 2008; Li et al., 2010). The euxinic ocean is rich in hydrogen sulfide (or sulfidic) in the water column, while the ferruginous ocean contains excessive dissolved ferrous Fe. Therefore, to better understand the deep oceanic changes during the E–C transition, we carried out high-resolution chemostratigraphic investigations in this study and presented more expanded and complete carbon and sulfur isotopic records and Fe speciation data in the deep-water E–C boundary succession (Liuchapo and Niutitang Formations) in western Hunan, South China (Fig. 1).

2. Geological setting and stratigraphy

During the E–C transition, the Yangtze block gradually evolved from a rift to a passive continental margin basin (Wang and Li, 2003). Carbonate platforms were developed on palaeohighs likely induced by block tilting in the context of extensional tectonism, which were surrounded by deeper siliceous slope-to-basinal environments

* Corresponding author.
E-mail address: dzh-chen@mail.iggcas.ac.cn (D. Chen).

0009-2541/$ – see front matter © 2012 Elsevier B.V. All rights reserved.
doi:10.1016/j.chemgeo.2012.03.005

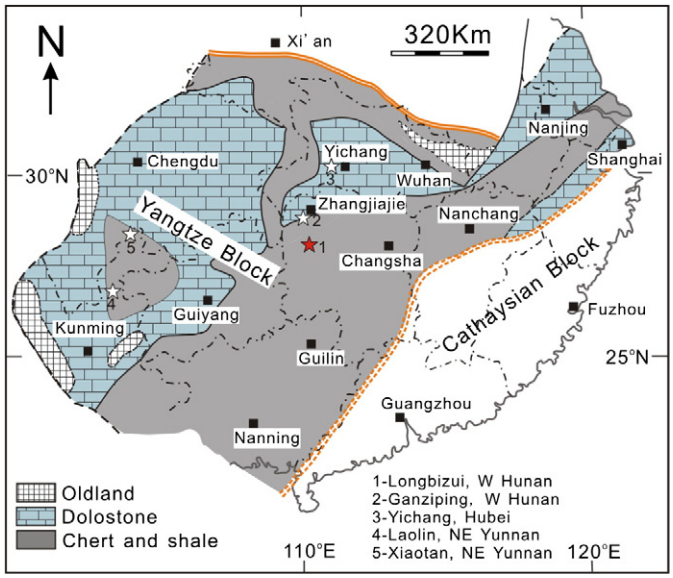

Fig. 1. Lithofacies paleogeographic map of Yangtze block during the Ediacaran–Cambrian transition. Note the deep-water depositional setting of studied section (Longbizui).

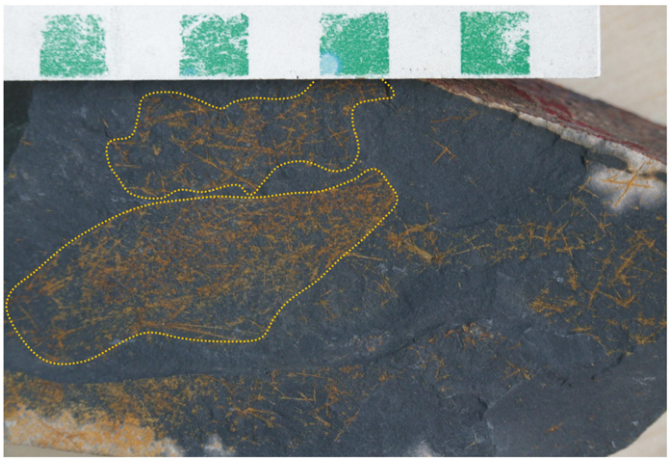

Fig. 2. Articulated sponge body (likely *Protospongia*) (within dashed line) and sponge spicules on the bedding planes of black shale from the upper section studied (see Fig. 3 for the stratigraphic occurrence). Scale bar equals 1 cm.

off the marginal zones (Fig. 1) (Chen et al., 2009; Wang et al., 2012). These platforms were subsequently drowned by a deep muddy shelf system in the Early Cambrian as a result of large-scale transgression (or relative sea-level rise) (e.g., Goldberg et al., 2007). The deep-water regimes were generally well connected outwards. In this study, a well-exposed outcrop section, located at Longbizui, Guzhang County in western Hunan, was selected for the chemostratigraphic study. Paleogeographically, it was located in the deep-water lower slope to basinal setting southeast of the Middle Yangtze Platform (Fig. 1) (e.g., Chen et al., 2009; Wang et al., 2012). At this locality, the E–C boundary succession, overlying the uppermost black shale of the Doushantuo Formation (Zhu et al., 2003), includes the Liuchapo and Niutitang Formations in ascending order. The Liuchapo Formation, equivalent of the shallow-water Dengying Formation (mostly dolostones), is composed of dark gray to black, thin- to medium-bedded chert deposits, locally intercalated with thin layers of black shales. The Niutitang Formation consists of a lower unit of siliceous-phosphorous shales (~10 m thick) with thin intercalations of phosphorite, and an upper thicker succession of black shale and mudstone. Sedimentological evidence for re-sedimentation by sediment gravity flow or contour currents is not observed. The Liuchapo Formation and the lower part of Niutitang Formation are generally fossil-poor. In contrast, the upper part of Niutitang Formation contains abundant sponges and/or sponge spicules, which likely belong to the *Protospongiidae* sp. (pers. comm. S. Xiao) (Fig. 2).

3. Methods

Fresh samples were collected and crushed into powder for analyses of total organic carbon (TOC), pyrite content, isotopic compositions of organic carbon ($\delta^{13}C_{org}$) and sulfide ($\delta^{34}S_{py}$), and Fe species.

Aliquots (200 mg) for TOC analysis were firstly treated with 10% (volume) hydrochloric acid (HCl) at 60 °C to remove carbonate, and then washed with distilled water to remove HCl. Afterwards, the samples were dried overnight (50 °C) and then analyzed using a LECO CS-400 analyzer. Sample splits (300 mg to 1.5 g) for $\delta^{13}C_{org}$ analysis were firstly dissolved with 6N HCl in a centrifuge beaker to remove carbonates. The decalcified samples (30–100 mg) + CuO wire (1 g) were added to a quartz tube, and combusted at 500 °C for 1 h and 850 °C for another 3 h. Isotopic ratios were analyzed using cryogenically purified CO_2 in a Finnigan MAT-253 mass spectrometer, and reported in standard δ-notation relative to Vienna Peedee Belmnite (VPDB) standard. Analytical precision for $\delta^{13}C_{org}$ is better than ±0.06‰. Pyrite extraction was carried out by using chromium reduction method (Canfield et al., 1986). Powdered samples (1–2 g) were reacted with 100 ml $CrCl_2$ + 10 ml alcohol solution. The liberated hydrogen sulfide was immediately purged by the N_2 stream, and was trapped and collected in the 2% $AgNO_3$ solution to precipitate Ag_2S, then filtered, rinsed, dried and weighed. The reproducibility of replicate analyses was generally better than 1%. The dried Ag_2S was mixed with V_2O_5 and combusted up to 1050 °C to convert to SO_2 gasses. Sulfur isotopic ratios were measured using purified SO_2 in the Finnigan Delta-S mass spectrometer, and reported in δ-notation relative to Canon Diablo Troilite (CDT) standard. The analytical precision is better than ±0.2‰.

The ocean redox states during the E–C transition are explored by the Fe speciation in the deep-water sediments. The highly reactive Fe (Fe_{HR}) is broadly apportioned into four different pools: carbonate Fe (Fe_{carb}), oxide Fe (Fe_{ox}), magnetite Fe (Fe_{mag}) and pyrite Fe (Fe_P); the sum of these pools represents the total concentration of highly reactive Fe ($Fe_{HR} = Fe_{carb} + Fe_{ox} + Fe_{mag} + Fe_{py}$) (Poulton and Canfield, 2005; Poulton and Canfield, 2011). Fe_{carb} was extracted from iron carbonate minerals with sodium acetate solution adjusted to pH = 4.5 by addition of trace-metal grade acetic acid; Fe_{ox} was extracted from iron oxide/oxyhydroxide phase using a 50 g/L sodium dithionite solution buffered to pH = 4.8 with 0.2 M sodium citrate and trace-metal grade acetic acid; Fe_{mag} was extracted from magnetite by a 0.2 M ammonium oxalate and 0.17 M oxalic acid solution. All extracts were diluted and then analyzed by atomic absorption spectroscopy for their Fe contents (Poulton and Canfield, 2005; Poulton et al., 2010). Fe_P was calculated by stoichiometry from Cr-reduction pyrite (Canfield et al., 1986). Fe_T was analyzed by automatic X-ray fluorescence spectrometer (XRF-1500) on fused glass disks. In this study, Fe_{HR}/Fe_T and Fe_P/Fe_{HR} ratios are used as the indicators of water column redox and sulfidicity, respectively (e.g., Poulton et al., 2004; Canfield et al., 2007, 2008; Poulton et al., 2010).

4. Results

Results of $\delta^{13}C_{org}$ and $\delta^{34}S_{py}$ as well as Fe species are given in Fig. 3 and Table 1. The $\delta^{13}C_{org}$ values generally vary from −37.31 to −32.75‰ VPDB (average −34.61‰) through Liuchapo to Niutitang Formations (Table 1), and four major positive (P1–P4) and negative (N1–N4) excursions are identified, of which the largest negative spike (N2) is pinned at the middle of Liuchapo Formation (at ~40 m) (Fig. 3). A less prominent positive shift (P5) can also be recognized in the mid-upper part of Niutitang Formation (at ~110–120 m) (Fig. 3). The $\delta^{34}S_{py}$ values vary in a wide range between −10.8 and

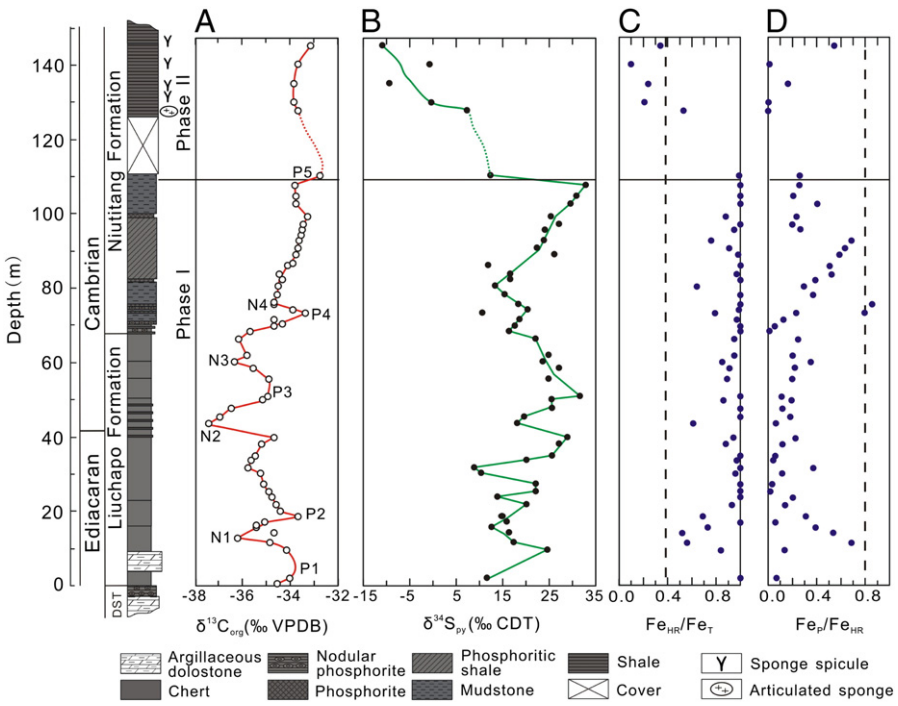

Fig. 3. Vertical variations in $\delta^{13}C_{org}$, $\delta^{34}S_{py}$ and Fe speciation across the E–C boundary succession (from Liuchapo to Niutitang Formations) at Longbizui section, western Hunan, South China. Dashed lines mark at 0.80 of Fe_P/Fe_{HR} ratio and 0.38 of Fe_{HR}/Fe_T ratio, respectively. DST, Doushantuo Formation.

33.0‰ CDT (average 18.5‰) (Table 1). Generally, the $\delta^{34}S_{py}$ values roughly follow the variation tracks of $\delta^{13}C_{org}$ values, showing, more or less, coupled carbon and sulfur cycling but decoupled at the upper part of the section (at ~110 m and farther upwards) by a sudden decrease in $\delta^{34}S_{py}$ values (Fig. 3).

Most samples, except two samples near the base of Niutitang black shales, have Fe_P/Fe_{HR} ratios lower than 0.80 (average 0.36), in which those in Liuchapo chert deposits are lower (average 0.19). On the other hand, most samples, except four samples in the uppermost of Niutitang black shale, have Fe_{HR}/Fe_T ratios ranging from 0.50 to 1.00, greater than 0.38 (Table 1; Fig. 3).

5. Discussion

5.1. Constraints on stratigraphic correlation

Owing to sparse availability of reliable biostratigraphic and radiometric dating data, the stratigraphic subdivision and correlation of deep-water E–C boundary strata with the shallow-water equivalents were not well constrained. Previous stratigraphic works have demonstrated that an organic-rich (TOC ≥ 10% locally) black shale horizon (generally <2 m thick) occurs across the boundary between Doushantuo and Liuchapo (or Dengying) Formations, and is widely traceable from the platform to the basinal successions (Zhu et al., 2003; Jiang et al., 2006; Chen et al., 2009); it is thus considered as the reliable basal marker bed of the E–C boundary successions in South China (Jiang et al., 2007a, 2007b). An age of 551.1 ± 0.7 Ma from this marker bed was determined by the U–Pb zircon age (Condon et al., 2005; Zhang et al., 2005). Above this horizon, whatever the deep-water Liuchapo chert deposits or the shallow-water Dengying carbonates, they all are overlain by the Niutitang Formation (black shale–mudstone series) of the Lower Cambrian (Zhu et al., 2003; Chen et al., 2009). A new SHRIMP U–Pb zircon age of 532.3 ± 0.7 Ma was determined in the lowermost black shale of the Niutitang Formation, i.e., in Guizhou Province, southwestern China (Jiang et al., 2009), which is apparently younger than the E–C boundary age of 542.0 ± 0.3 Ma (Amthor et al., 2003). In view of more continuous deposition in the deep-water slope-to-basin setting, the E–C boundary thus should be logically placed at a level within the Liuchapo Formation. This placement is consistent with the case that the small shelly fossils (SSFs), the indicator for the approximate onset of Cambrian (Steiner et al., 2007), locally occur in the more muddy part of the uppermost Liuchapo chert (Qian and Yin, 1984). This further affirms that the deep-water Liuchapo Formation straddles across the E–C boundary, although the exact placement is waiting for further confirmation.

In general, the lower part of Niutitang Formation (or equivalents) bears a very few fossils. However, the upper part of Niutitang Formation (or equivalents) commonly contains relatively abundant fossils, i.e., the assemblage of hexactinellid sponges and questionable demosponges, and some organic tissues and mineralized spicules in Hunan (Steiner et al., 2005), eodiscid trilobites *Hubeidiscus*, *Sinodiscus* and *Megaredlichia* in Guizhou (Yang et al., 2003), and trilobites such as *Hunanocephalus*, *Hupeidiscus*, and *Hsuaspis* in Anhui and Zhejiang (Li et al., 1990; He and Yu, 1992), thus this horizon is proposed to be correlated approximately with the Atdabanian stage (Stage 3) (e. g, Yuan et al., 2002; Steiner et al., 2005; Goldberg et al., 2007). In this context, the lower part of Niutitang Formation should be placed immediately below the Atdabanian stage (Stage 3), within the Tommotian stage (Stage 2), based on the vertical stacking relationship. The radiometric age derived from this interval, as documented above, also reconcile this placement.

At studied section, abundant sponges and/or sponge spicules occur in the upper Niutitang Formation which are probably correlated temporally with the Chengjiang-type fauna in southwestern China (e.g., Steiner et al., 2005) (Fig. 3). Thus it is reasonable to correlate this horizon with the Atdabanian as well. In summary, as a whole, the E–C succession from the Liuchapo Formation to the upper fossil-bearing Niutitang Formation are supposed to span from the terminal Ediacaran (~551 Ma) to the Atdabanian in the Early Cambrian. Carbon isotope chemostratigraphy can provide further constraints on the stratigraphic divisions within this succession and their correlation.

Carbon isotopic chemostratigraphy have been proven as a powerful tool for the global correlation, particularly in the fossil-deficient Neoproterozoic-Cambrian successions (e.g., Knoll and Walter, 1992;

Table 1
$\delta^{13}C_{org}$, $\delta^{34}S_{py}$ and Fe speciation data across the E–C boundary succession (from Liuchapo to Niutitang Formations) at Longbizui, western Hunan, South China.

	Sample	Depth (m)	$\delta^{13}C_{org}$ (‰ VPDB)	$\delta^{34}S_{py}$ (‰ CDT)	TOC (wt.%)	Pyrite (wt.%)	S_{py}/TOC	Fe_T (wt.%)	Fe_{oxide} (wt.%)	Fe_{carb} (wt.%)	Fe_{mag} (wt.%)	Fe_p (wt.%)	Fe_{HR} (wt.%)	Fe_P/Fe_{HR}	Fe_{HR}/Fe_T
Niutitang Formation	LBZ-103	145.2	−33.13	−10.8	0.58	1.83	1.68	4.66	0.56	0.09	0.07	0.85	1.57	0.54	0.34
	LBZ-102	140.2	−33.65	−0.8	1.23	<0.01	<0.01	0.83	0.07	<0.01	0.01	<0.01	0.08	0.01	0.10
	LBZ-101	135.1	−33.84	−9.2	1.46	0.08	0.03	0.97	0.17	0.01	0.01	0.04	0.23	0.16	0.24
	LBZ-100	130.1	−33.83	0.3	0.89	<0.01	<0.01	0.84	0.17	<0.01	0.01	<0.01	0.17	<0.01	0.21
	LBZ-99	127.8	−33.65	7.5	1.38	<0.01	<0.01	1.02	0.53	<0.01	0.01	<0.01	0.54	<0.01	0.53
	LBZ-98	110.4	−32.75	12.5	4.82	0.78	0.09	1.41	1.02	<0.01	0.02	0.37	1.40	0.26	0.99
	LBZ-96	107.6	−33.76	33.0	5.39	0.35	0.03	0.62	0.45	<0.01	0.02	0.16	0.64	0.26	1.04
	LBZ-94	104.8	−33.76	31.0	5.26	1.23	0.13	2.73	1.41	0.65	0.11	0.58	2.74	0.21	1.00
	LBZ-93	102.7	−33.76	29.6	6.82	2.69	0.21	2.84	1.08	0.66	0.11	1.25	3.10	0.40	1.09
	LBZ-91	99.2	−33.33	25.5	8.19	0.53	0.03	1.21	0.70	0.08	0.03	0.25	1.06	0.23	0.88
	LBZ-89	97.1	−33.45	27.4	7.08	1.51	0.11	2.53	1.86	0.89	0.12	0.70	3.57	0.20	1.41
	LBZ-88	95.7	−33.47	24.2	6.34	0.49	0.04	0.90	0.51	0.06	0.06	0.23	0.86	0.27	0.95
	LBZ-84	94.4	−33.54												
	LBZ-82	92.9	−33.62	24.0	6.50	3.37	0.28	3.00	0.55	0.13	0.05	1.57	2.29	0.69	0.76
	LBZ-80	90.9	−33.66	22.5	2.52	0.90	0.19	0.73	0.22	0.01	0.02	0.42	0.67	0.63	0.91
	LBZ-78	89.1	−33.73	26.4	6.62	2.76	0.22	2.25	0.76	0.08	0.06	1.29	2.19	0.59	0.98
	LBZ-76	86.8	−33.87												
	LBZ-75	86.1	−34.11	11.9	6.19	2.06	0.18	1.62	0.84	0.04	0.06	0.96	1.89	0.51	1.17
	LBZ-73	83.9	−34.44	16.7	6.00	1.64	0.15	1.51	0.65	0.01	0.03	0.77	1.47	0.52	0.97
	LBZ-71	82.5	−34.32	16.8	7.09	2.56	0.19	2.72	1.36	0.42	0.11	1.19	3.08	0.39	1.13
	LBZ-69	80.7	−34.47	13.5	7.13	1.19	0.09	2.95	1.07	0.16	0.11	0.55	1.89	0.29	0.64
	LBZ-67	78.3	−34.52	15.5	8.94	2.98	0.18	3.40	1.84	0.39	0.12	1.39	3.74	0.37	1.10
	LBZ-64	76.2	−34.64												
	LBZ-63	75.7	−34.65	18.6	6.60	5.86	0.47	2.81	0.32	0.09	0.04	2.74	3.18	0.86	1.13
	LBZ-59	74.2	−33.88	20.5	3.71	0.14	0.02	0.29	0.20	<0.01	0.01	0.07	0.28	0.23	0.99
	LBZ-57	73.4	−33.37	10.7	8.98	3.96	0.24	2.93	0.44	0.02	0.01	1.85	2.40	0.80	0.79
	LBZ-54	71.6	−34.65	18.8	4.30	0.07	0.01	0.27	0.21	<0.01	0.02	0.03	0.26	0.13	0.97
	LBZ-53	70.5	−34.31												
Liuchapo Formation	LBZ-49	69.9	−34.63	17.7	1.31	0.02	0.01	0.20	0.19	<0.01	0.02	0.01	0.22	0.05	1.12
	LBZ-47	68.5	−35.66	16.6	1.62	0.01	<0.01	0.25	0.23	0.06	0.02	<0.01	0.32	0.01	1.29
	LBZ-46	66.3	−36.14	22.2	1.37	0.17	0.07	0.34	0.22	<0.01	0.02	0.08	0.32	0.25	0.95
	LBZ-45	61.9	−35.76	24.9	0.56	0.15	0.14	0.37	0.27	<0.01	0.01	0.07	0.35	0.20	0.95
	LBZ-44	60.2	−36.29	23.8	1.27	0.28	0.12	0.44	0.21	0.01	0.02	0.13	0.38	0.35	0.85
	LBZ-43	58.5	−35.51	27.3	0.82	0.19	0.13	0.46	0.29	0.01	0.02	0.09	0.41	0.22	0.91
	LBZ-42	55.6	−34.88	25.1	0.98	0.18	0.10	0.47	0.32	0.01	0.01	0.08	0.42	0.20	0.89
	LBZ-41	50.9	−34.89	31.6	0.88	0.16	0.10	0.67	0.53	0.02	0.04	0.08	0.67	0.11	1.00
	LBZ-40	49.9	−35.14	25.3	1.17	0.21	0.10	0.60	0.39	<0.01	0.02	0.10	0.51	0.19	0.86
	LBZ-39	47.8	−36.42	25.8	1.37	0.10	0.04	0.40	0.33	<0.01	0.03	0.05	0.40	0.12	1.01
	LBZ-38	45.5	−36.93	19.7	2.16	0.12	0.03	0.31	0.25	<0.01	0.01	0.06	0.31	0.18	1.01
	LBZ-37	43.5	−37.31	18.2	2.26	0.14	0.03	1.70	0.79	0.11	0.07	0.07	1.04	0.06	0.61
	LBZ-36	39.9	−34.64	28.9	0.70	0.25	0.19	0.55	0.37	<0.01	0.03	0.12	0.52	0.22	0.94
	LBZ-35	38.2	−35.19	27.2	1.07	0.12	0.06	0.54	0.38	<0.01	0.04	0.06	0.47	0.12	0.88
	LBZ-34	35.1	−35.43	25.8	4.04	0.04	<0.01	0.27	0.26	<0.01	0.02	0.02	0.29	0.06	1.08
	LBZ-33	33.9	−35.62	20.2	5.02	0.03	<0.01	0.32	0.29	<0.01	0.01	0.01	0.31	0.04	0.97
	LBZ-32	31.7	−35.73	8.9	6.79	0.87	0.07	1.06	0.64	<0.01	0.05	0.41	1.10	0.37	1.04
	LBZ-31	30.3	−35.23	10.6	1.48	0.07	0.03	0.31	0.25	<0.01	0.02	0.03	0.30	0.11	0.96
	LBZ-30	27.4	−35.10	22.3	5.35	0.04	<0.01	0.53	0.54	<0.01	0.01	0.02	0.57	0.03	1.08
	LBZ-29	25.4	−34.88	22.2	1.14	0.03	0.01	0.66	0.64	<0.01	0.06	0.01	0.71	0.02	1.08
	LBZ-28	23.9	−34.74	14.1	0.94	0.25	0.14	0.55	0.42	<0.01	0.03	0.12	0.58	0.20	1.05
	LBZ-27	22.0	−34.58	20.2	0.50	0.16	0.17	0.57	0.42	<0.01	0.04	0.07	0.53	0.14	0.93
	LBZ-26	20.2	−34.41												
	LBZ-25	18.6	−33.67	15.1	0.13	0.63	2.60	1.37	0.61	<0.01	0.05	0.30	0.95	0.31	0.69
	LBZ-24	17.1	−35.02	16.1	0.54	0.07	0.07	0.46	0.44	<0.01	0.04	0.03	0.51	0.06	1.11
	LBZ-23	16.2	−35.39												
	LBZ-22	15.6	−35.40	12.8	0.78	0.39	0.26	0.64	0.25	0.01	0.03	0.18	0.46	0.39	0.73
	LBZ-21	14.2	−34.65	16.5	0.15	0.50	1.78	0.84	0.19	<0.01	0.02	0.23	0.44	0.54	0.52
	LBZ-20	12.9	−36.18												
	LBZ-19	11.7	−34.81	17.5	0.13	0.67	2.75	0.82	0.13	<0.01	0.01	0.31	0.46	0.69	0.56
	LBZ-17	9.7	−34.15	24.9	1.95	0.07	0.02	0.29	0.19	<0.01	0.02	0.03	0.24	0.13	0.84
	LBZ-16	2.0	−34.02	11.8	0.19	0.05	0.15	0.34	0.30	<0.01	0.02	0.02	0.35	0.07	1.05
	LBZ-14	0.7	−34.51												

Kaufman and Knoll, 1995; Brasier et al., 1996; Shen and Schidlowski, 2000; Corsetti and Hagadorn, 2000; Ishikawa et al., 2008). Previous researches demonstrated several isotopic perturbations of, although mostly carbonate carbon, which are commonly coincident with stratigraphic formation (or member) boundaries within the E–C successions (e.g., Zhou et al., 1997; Shen and Schidlowski, 2000; Kimura and Watanabe, 2001). Due to the absence of carbonates across the deep-water E–C succession at studied section, $\delta^{13}C_{carb}$ data are thus not available. In this case, $\delta^{13}C_{org}$ data, which generally vary in parallel with $\delta^{13}C_{carb}$ data in Phanerozoic times (e.g., Kump and Arthur, 1999; Shen and Schidlowski, 2000; Kimura and Watanabe, 2001), are thus exclusively used to characterize the further stratigraphic divisions and their correlation with shallow-water equivalents in South China and elsewhere over the world.

The weak, but positive correlation between $\delta^{13}C_{org}$ and TOC data (Fig. 4) indicates that the $\delta^{13}C_{org}$ variations at this locality were not caused by differential thermal alterations of organic matter during diagenesis; if so a negative covariance between them would be indicated since sparsely-distributed organic matter in sediments was more readily subject to thermal alteration, leading to heavier $\delta^{13}C_{org}$

values by removing the ^{12}C-enriched carbon (e.g., Hayes et al., 1999; Kump et al., 1999). Moreover, previous study showed that the H/C ratios of organic matter in the Liuchapo and Xiaoyanxi (equivalent of Niutitang) Formations vary between 0.3 and 1.8 at Yanwutan–Lijiatuo section not far from the studied section in western Hunan Province (Guo et al., 2007), implicating that the $\delta^{13}C_{org}$ values at that area were not significantly affected by thermal maturation as well. Even if the studied succession was subject to postdepositional thermal alteration, the influence is assumed to be basically uniform throughout the section, in view of such a short stratigraphic interval. Furthermore, the independence of $\delta^{13}C_{org}$ variations from the lithologies also suggests that the primary signatures of $\delta^{13}C_{org}$ variations were basically preserved in the deposits.

As discussed above, the base of the deep-water Liuchapo Formation is synchronously correlated with the base of the shallow-water Dengying Formation in South China. Two positive $\delta^{13}C$ excursions (A1 and A2) in the lower part, followed by, more or less, a persistent pattern, had been reported in the Dengying Formation, i.e., at Yichang, South China (e.g., Lambert et al., 1987). Coincidently, two positive $\delta^{13}C_{org}$ shifts (P1 and P2) were also recognized in the lower part of Liuchapo Formation at studied section, thus they are suggested to be reasonably correlated with those in the Dengying Formation at Yichang (Fig. 5).

An apparent large $\delta^{13}C$ negative excursion, calibrated with the first appearance of SSFs, has been proposed as the approximate beginning of Cambrian, which is placed at or near the base of the Nemakit–Daldynian Stage (or Stage 1) (e.g., Kaufman et al., 1996; Steiner et al., 2007). In the basal Cambrian shallow-water successions of South China, three negative $\delta^{13}C$ excursions (N1–N3 at Ganziping, A–C at Laolin) and two interjacent positive excursions (P1 and P2 at Ganziping, S2 and S3 at Laolin) were revealed from the base of Cambrian to the base of Shiyantou Member (or Niutitang Formation) (Zhou et al., 1997; Shen and Schidlowski, 2000; Chen et al., 2009). Coincidently, three negative (N2 to N4) and two interjacent positive $\delta^{13}C_{org}$ excursions (P3 and P4) were revealed from the middle of Liuchapo Formation (at depth of ~40 m) to the base of Niutitang Formation at Longbizui, which can be correlated one by one with the $\delta^{13}C$ perturbations in equivalent shallow-water deposits (Fig. 5). In this case, the large negative $\delta^{13}C_{org}$ excursion (N2) in the middle of Liuchapo Formation is accordingly considered to be correspondent to the negative anomaly between the Baiyanshao and Xiaowaitoushan Members that marks the first appearance of SSFs (Chinese Marker A), the proposed E–C boundary in South China (Zhou et al., 1997; Shen and Schidlowski, 2000; Steiner et al., 2007). This negative excursion is also apparent on Siberian platform (Brasier et al., 1994; Kaufman et al., 1996), in Morocco (Maloof et al., 2010) and elsewhere. Above this large negative isotopic excursion (N2), two positive isotopic shifts in the upper part of Liuchapo Formation (P3) and in the base of Niutitang Formation (P4) accordingly are correlated with the two isotopic peaks in the upper part of Xiaowaitoushan and middle part of Dahai Members, respectively, in northeastern Yunnan, southwestern China; they are further proposed to be correlated with the two isotopic peaks Z and I in Siberia, two peaks I and I' in Morocco (Fig. 5), constrained by similar fossil assemblages. The subsequent negative excursion (N4) in the lower part of Niutitang Formation is then propose to be correlated with that in the base of Shiyantou Member in northeastern Yunnan (Zhou et al., 1997) and with that in the base of Tommotian (or Stage 2) elsewhere (Brasier et al., 1994; Maloof et al., 2010). Further upwards, the uppermost carbon isotopic peak (P5) at this section is likely correlated with the isotopic peak in the base of Yu'anshan Member, southwestern China (Zhou et al., 1997) or elsewhere in the base of Atdabanian (or Stage 3) (Brasier et al., 1994; Maloof et al., 2010). The abrupt appearance of abundant large-body sponges in this horizon as mentioned above also reconciles this correlation.

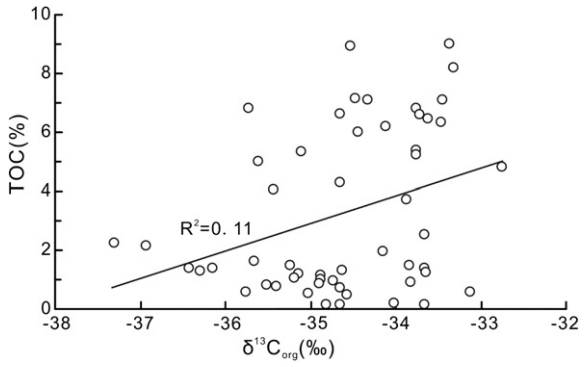

Fig. 4. Crossplot of $\delta^{13}C_{org}$ values and organic abundance (TOC), very weak positive relationship is present between them.

5.2. Deep oceanic redox condition

Oceanic redox conditions can be well evaluated by Fe speciation (e.g., Poulton et al., 2004; Canfield et al., 2008; Johnston et al., 2010; Poulton et al., 2010; Gill et al., 2011). The data presented here approximately reveal two major phases (Phases I and II) of ocean evolution in redox condition during the E–C transition, which is demarcated at depth of 110 m in the upper part of Niutitang Formation (Fig. 3), corresponding to the onset of Atdabanian (or Stage 3; Fig. 5) as documented above. Phase I is characterized by relatively high Fe_{HR}/Fe_T ratios (all >0.38) and low Fe_P/Fe_{HR} ratios (mostly <0.80 except for two samples in the base of Niutitang Formation); while phase II is characterized by rapid decreases in Fe_{HR}/Fe_T ratio (<0.38).

In modern marine sediments deposited under oxic waters, Fe_{HR} constitutes a maximum of 38% of the Fe_T pool; in contrast, sediments deposited under anoxic waters, can have much higher proportion of Fe_{HR} (Raiswell and Canfield, 1998). Thus, when ratios of Fe_{HR}/Fe_T exceed 0.38, deposition from anoxic bottom waters is indicated, and vice versa. Furthermore, ratios of Fe_P/Fe_{HR} in sediments are further used to explore the nature of anoxic deep waters (i.e., availability of iron vs. sulfur). Under sulfidic water conditions, ratios of Fe_P/Fe_{HR} in sediments commonly exceed 0.80; under anoxic, ferruginous water columns, however, they are lower than 0.80 (Poulton et al., 2004; Canfield et al., 2008).

During phase I, all ratios of Fe_{HR}/Fe_T in both chert and shale exceed 0.38 (mostly >0.70), providing compelling evidence of deep ocean anoxia. Meanwhile, most of the ratios of Fe_P/Fe_{HR} are lower than 0.80 except for two samples in the lower part of Niutitang Formation (Fig. 3), indicating a predominance of anoxic and ferruginous ocean, only punctuated temporarily by a sulfidic episode in the earliest Cambrian. The same pattern can be seen at Songtao section, Guizhou province (Canfield et al., 2008). A widespread polymetallic Ni–Mo–PGE–Au sulfide orebed (generally 1–10 cm thick) was deposited mostly along the antecedent platform margin, South China during the earliest Niutitang time (Jiang et al., 2007a, 2007b; Chen et al., 2009), indicating a transient sulfide boost in the water column. Thus, this short sulfidic episode at studied section is supposed to correspond to which the extensive polymetallic sulfide orebed was deposited in South China. This scenario, to some extent, reconciles the Mo isotopic evidence from Wille et al. (2009), although their claim for a predominance of sulfidic ocean over the Early Cambrian is purported due to the poor constraint on timing (Jiang et al., 2009). It is also noted that, although an anoxic, ferruginous deep sea as indicated by ratios of Fe_{HR}/Fe_T predominated over the Yangtze area, an increase trend of sulfide (thereby sulfate) concentration in water column, as shown by ratios of Fe_P/Fe_{HR}, did occur notably during late phase I (mostly in the early Niutitang time) (Fig. 3), indicating that the

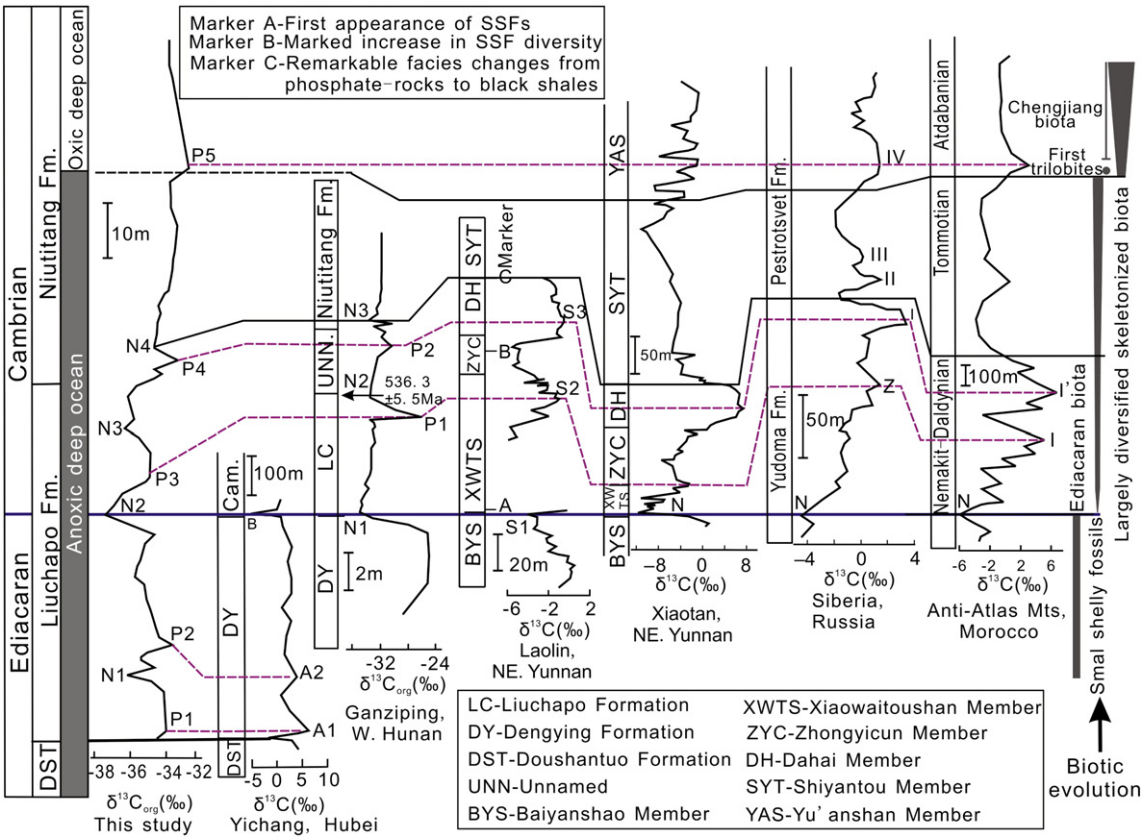

Fig. 5. Carbon isotopic variations across the E–C transition at Longbizui, Guzhang County, western Hunan, and their correlation with those at Yichang (Lambert et al., 1987), Ganziping (Chen et al., 2009), Laolin (Shen and Schidlowski, 2000) and Xiaotan (Zhou et al., 1997) in South China (see Fig. 1 for locations), in Siberia, Russia (Brasier et al., 1994) and Anti-Atlas Mountains, Morocco (Maloof et al., 2010). Note the oceanic evolution (left) and simplified coeval biotic evolution (right).

deep oceanic state was not persistently stable but fluctuating prior to oxygenation.

During phase II, the Fe_{HR}/Fe_T ratios, although not densely controlled due to outcrop quality, apparently drop down to the values lower than 0.38 near the top of section (Fig. 3), suggesting that the deep ocean was quickly transferred into an oxic ocean during the Atdabanian. This scenario is further supported by the abrupt occurrence of abundant sponges and/or sponge spicules in the deposits (Fig. 2). Although sea level fall and/or enhanced bottom water current (i.e., turbidite flow) could have induced local improvement in water ventilation (or oxygenation), no sedimentological evidence is available for supporting such a scenario as documented above. On the other hand, the widespread presence of articulate sponges (Fig. 2) does not support strong bottom water reworking as well. The rapid oxygenation and/or well-improved ventilation in the deep ocean further indicate a greatly increased oxygen level in the ocean–atmosphere system during this interval.

5.3. Sulfate concentration during the E–C transition

The sulfate level in seawater is the principal factor controlling the bacterial sulfate reduction (BSR) on Earth's surface (e.g., Canfield, 2004). The $\delta^{34}S_{py}$ values of pyrite precipitated in water media are dependent on the fractionation of BSR; the extent to which the fractionation occur between seawater sulfate and BSR-induced sedimentary pyrite is largely controlled by sulfate availability (Habicht et al., 2002; Hurtgen et al., 2009). The seawater sulfate concentration, in turn, is a reflection of oxygen level in the ocean–atmosphere system because the primary source of seawater sulfate from riverine input results in most part from the weathering oxidation of pyrite (e.g., Canfield, 2004).

In the anoxic phase I (late Ediacaran through Tommotian), $\delta^{34}S_{py}$ values vary from 8.9 to 33.0‰ CDT (average 20.9‰) (Table 1; Fig. 3). Given a probable sulfur isotopic value of seawater sulfate around 25–35‰ during the terminal Neoproterozoic to the Early Cambrian (Strauss, 1997; Shen et al., 1998; Goldberg et al., 2005), more than half of samples yield $\delta^{34}S_{py}$ values close to the $\delta^{34}S_{sulfate}$ values of coeval seawater, implicating a relative low seawater sulfate concentration, at least, in this deep basin. This scenario also reconciles a ferruginous-dominated ocean revealed by Fe speciation (e.g., Canfield et al., 2008; Li et al., 2010) as documented above. However, the seawater sulfate concentration may have not been persistently low, rather, fluctuating as indicated by the frequent negative shifts of $\delta^{34}S_{py}$ values in the deep ocean during the E–C transition. In a longer-term view, the negative excursions are more prominent, notably in the lower parts of both Liuchapo and Niutitang Formations, suggesting an increase in seawater sulfate level during the two intervals; this scenario is further confirmed by the coeval increases in Fe_p/Fe_{HR} ratios as documented above (Fig. 3).

Although some studies suggested an increase in seawater sulfate availability as a consequence of enhanced oxygenation of the ocean–atmosphere system during the E–C transition (Canfield and Teske, 1996; Hurtgen et al., 2005; Fike et al., 2006; Halverson and Hurtgen, 2007; McFadden et al., 2008). However, many other studies have also revealed a low sulfate concentration throughout the E–C transition as for the relatively enriched $\delta^{34}S_{py}$ values (Bottomley et al., 1992; Strauss et al., 1992; Ries et al., 2009). This paradox may result from the spatial heterogeneity of seawater sulfate concentration which was relatively high in the nearshore subbasins close to the riverine sources, and low in the offshore deeper subbasins away the sources (e.g., Li et al., 2010; Poulton et al., 2010). In this case, the sulfate concentration in the oceanic basin during the E–C transition, as a

whole, was also probably not persistent laterally and different from the case in the modern ocean.

During phase II (Atdabanian or Stage 3), $\delta^{34}S_{py}$ values decrease abruptly from 33.0 to −10.8‰ (Fig. 3). The lower $\delta^{34}S_{py}$ values (average −0.1‰), in comparison with those of phase I (average 20.9‰), likely reflect the largely increased BSR-mediated sulfur isotopic fractionation; this scenario could have resulted from a rapid increase in sulfate concentration in the ocean as a consequence of increased oxygen concentration (e.g., Habicht et al., 2002). This is consistent with the state of oxic deep sea unraveled by a rapid decrease in Fe_{HR}/Fe_T ratio as documented above. Although sea level fall and/or enhanced bottom water flow on the slope may have resulted in similar outcome through increased downward diffusion of sulfate into sediments underneath, this is not supported by the sedimentological evidence.

5.4. Carbon and sulfur cycling during the E–C transition

As documented above, the $\delta^{13}C_{org}$ values were quite fluctuating in deep sea from the latest Ediacaran through Early Cambrian. This pattern is different from the scenario of earlier Doushantuo time (635 to 551 Ma). During that interval, $\delta^{13}C_{org}$ values were persistent, although $\delta^{13}C_{carb}$ values were fluctuating, based on which it was suggested that there was possibly a large dissolved organic (DOC) pool decoupled with the dissolved inorganic (DIC) pool owing to a very low oxygen concentration in the deep sea (e.g., McFadden et al., 2008). By contrast, the fluctuating pattern of $\delta^{13}C_{org}$ variations implicates a large-scale shrinkage of DOC pool, which was basically coupled with the DIC pool, in the deep sea later on, as the common scenario seen in Phanerozoic times (e.g., Kump and Arthur, 1999).

The coupling between $\delta^{13}C_{org}$ and $\delta^{34}S_{py}$ values, although with differential magnitudes, can be roughly recognized in the anoxic phase I (Fig. 3), suggesting that the residence time of DIC and sulfate may have been approximately comparable (e.g., Hurtgen et al., 2009), at least, in this basin. On the other hand, this approximate parallel variation pattern may still reflect the comparative small reservoirs of both sulfate and DIC in the E–C ocean (e.g., Bartley and Kah, 2004; Gill et al., 2007), although no isotopic data of DIC carbon and sulfate sulfur are available in this deep-water basin.

The positive $\delta^{13}C_{org}$ excursions are attributed to enhanced marine primary productivity and subsequent burial of organic matter, which preferentially removed the light isotope ^{12}C from the oceanic carbon reservoir (Kump and Arthur, 1999; Jiang et al., 2010). In this case, with largely increased input of labile organic matter, dissolved sulfate pool will have been progressively enriched in heavy isotope ^{34}S due to enhanced BSR activity. As the sulfate concentration falls below a threshold level (i.e., <200 μm), bacteria would lose their ability preferentially to remove the light isotope ^{32}S from the sulfate pool, driving isotopic composition of resulting pyrite to be heavier and heavier in a relative small sulfate reservoir in the deep ocean (Habicht et al., 2002). A similar pattern can be seen in the early Cambrian at Shatan section, NE Sichuan Province (Goldberg et al., 2007).

As for the concurrent negative excursions of $\delta^{13}C_{org}$ and $\delta^{34}S_{py}$, ocean overturning (e.g., Kimura et al., 1997) could lead to a negative $\delta^{13}C$ excursion through upwelling of massive ^{12}C-enriched deep waters into shallow waters. But this process would simultaneously drive the ^{34}S-enriched deep waters (e.g., Sælen et al., 1993) upward into shallow waters. Under this circumstance, the BSR-mediated pyrite would precipitate and inherit the signals of heavy isotopes from the sulfate, resulting in a positive excursion of $\delta^{34}S_{py}$ in a relative small sulfate reservoir; this scenario is apparently against the fact observed. In addition, releasing of methane hydrates into ocean even atmosphere could also cause negative swings of $\delta^{13}C_{org}$ values (Kimura and Watanabe, 2001), but this process was not necessarily tied to negative $\delta^{34}S_{py}$ excursions either.

An anoxic, ferruginous-dominant deep ocean during the E–C interval indicates an excess of Fe ion after pyrite formation in marine waters, which could have been augmented by hydrothermal venting (Canfield et al., 2008; Li et al., 2010; Poulton and Canfield, 2011). Hydrothermal venting has also been proposed to be responsible for the formation of Liuchapo chert deposits on platform marginal zones and possibly further basinward (Chen et al., 2009; Wang et al., 2012) and the formation of metalliferous (Ni–Mo–PGE) sulfides in the basal Niutitang black shales in South China (Steiner et al., 2001; Jiang et al., 2007a, 2007b). Numerous studies showed hydrothermal venting can release vast amounts of CO_2 and/or CH_4 (Charlou et al., 2002) which are characterized by isotopically extremely light carbon, and reduced sulfur species (mainly H_2S and SO_2; $\delta^{34}S = 0$ to 8‰) into oceans (e.g., Herzig et al., 1998). These gasses (including CH_4 and H_2S) would be oxidized directly into CO_2 and SO_4^{2-} with no isotopic fractionation, and then would be recycled by microorganisms in the oceanic C–S system. The increased fluxes of these isotopically light carbon and sulfur from hydrothermal venting could readily cause negative isotopic excursions of both carbon and sulfur in relative small reservoirs of both DIC and sulfate in sea waters. Multiple coupled negative excursions of $\delta^{13}C_{org}$ and $\delta^{34}S_{py}$, could thus indicate multiple episodes of hydrothermal activities in the basin during the E–C transition (e.g., Chen et al., 2009; Wang et al., 2012); the differences in the magnitude of C–S anomalies may have resulted from differential inputs of hydrothermally-originated C–S sources. However, as documented above, the longer-term negative $\delta^{34}S_{py}$ excursions may have not simply resulted from hydrothermal activities.

During phase II (Atdabanian or Stage 3), carbon and sulfur cycling was apparently decoupled as indicated by a large-scale, rapid decrease in $\delta^{34}S_{py}$ value with only a slight variation in $\delta^{13}C_{org}$ value (Fig. 3). The decoupling of C–S cycling was possibly related to the differential variations in pool size of DIC and sulfate, in which the latter was apparently enlarged with respect to the former. In this case, the BSR was greatly enhanced, leading to a rapid decrease in $\delta^{34}S_{py}$ value as observed. This case is also in agreement with an apparent rise in oxygen level in the deep ocean as revealed by Fe speciation as documented above.

Prior to this phase, the long-lasting anoxic and ferruginous-dominant ocean, could have provided enough bio-limiting nutrient Fe to sustain the persistent bloom of marine microorganisms (or phytoplankton) in surface waters, thereby greatly increasing the primary production and organic export (or burial) (Kolber et al., 1994; Behrenfeld et al., 1996; Falkowski et al., 1998). On the other hand, the anoxic, ferruginous but sulfate-poor ocean could have reduced the BSR-mediated consumption of organic matter, thereby enhancing the preservation of organic matter (Yan et al., 2012). The cumulatively increased net burial of organic carbon, in turn, could have decreased the CO_2 level (or climate cooling) and simultaneously increased the O_2 level in the atmosphere (Cooper et al., 1996; Berner and Petsch, 1998; Holland, 2006), ultimately leading to the complete oxygenation of deep ocean as seen in phase II, through enhanced exchanges between surface and deep waters or oceanic circulation due to climate cooling. On the other hand, the long-term trend of $\delta^{13}C_{org}$ increases, although episodic, notably from the beginning of Cambrian (N2 in the middle Liuchapo Formation; Fig. 3), reflects a progressive decrease in carbon isotope fractionation during photosynthetic carbon-fixation of microorganisms (or phytoplankton) in surface waters, also reconciling the progressive drop of CO_2 level in atmosphere and waters (Dean et al., 1986; Popp et al., 1989; Freeman and Hayes, 1992; Kump and Arthur, 1999).

5.5. Implication for the metazoan diversification in the Early Cambrian

The “Cambrian explosion” is perhaps the most significant evolutionary event recorded in the fossil records, and numerous explanations for this bioradiation have been provided from different

disciplines (Knoll and Carroll, 1999; Marshall, 2006; Erwin et al., 2011). Here we focus on the oceanic redox changes in the Early Cambrian and their possible linkage to the great biotic diversification. At studied section, the carbon–sulfur isotopic and Fe speciation data reveal that oxygenation of deep sea and the sudden appearance of large-body sponge fauna co-occurred during the Atdabanian (or Stage 3), suggesting a causal link between them.

In South China, the sudden appearance of large-body sponge fauna, although tiny-sized forms (<1 mm in size) could have occurred earlier locally (Li et al., 1998), was commonly considered to be taken place temporally in the Qingzhusi Stage (or Atdabanian) in view of their co-occurrences with the Chengjiang Biota, especially in relatively shallow-water settings (Zhang and Pratt, 1994; Steiner et al., 2005; Xiao et al., 2005; Zhao and Li, 2006). Therefore, the sudden appearance of large-body sponge fauna is also considered as the main course of the 'Cambrian Explosion' in South China and elsewhere (Xiao et al., 2005). In this case, the oxygenation process of deep sea was temporally correlated with the sudden appearance of larger, taxonomically- and morphologically-diversified skeletonized animals; they are exemplified by the Chengjiang Biota that colonized in shallow water regimes during the middle Early Cambrian (Atdabanian or Stage 3) in southwestern China, and are regarded as the first window of exceptional preservation of typical Phanerozoic taxa (Babcock et al., 2001; Hou et al., 2004; Fig. 5).

The presence of surplus free oxygen on Earth's surface is commonly regarded as the critical trigger that stimulated the diffusion-dependent aerobic metabolism (or respiration) of organisms in Earth's early history for its more effective approach to obtain the energy to sustain cell activity (Nursall, 1959; Raff and Raff, 1970). Therefore, the significant rise of oxygen, likely to a tipping point, in atmosphere and oceans in the middle Early Cambrian, as symbolized by the full oxygenation of deep ocean (Fig. 3), could have provided ever yet the most favorable environmental (or ecological) opportunity and greatly enhanced diffusion-dependent respiration and subsequent developmental (or genetic) innovation of some organisms with poor-developed respiratory and ventilatory systems, thereby triggering the rapid taxonomic diversification, body-plan complexation and gigantism of skeletonized metazoans (Raff and Raff, 1970; Graham et al., 1995; Knoll and Carroll, 1999; Erwin et al., 2011). Moreover, the boost of oxygen concentration in aquatic system could have increased oxygen penetration into dwelling substrates and resource accessibility or availability (Graham et al., 1995), enabling greater ecological exploitation, innovation and radiation (Logan et al., 1995; Knoll and Carroll, 1999; Butterfield, 2007; Erwin et al., 2011), thereby fuelling the diversification and ecological radiation of some taxa.

In contrast, prior to this full oxygenation, the predominance of anoxic deep ocean indicates that the oxygen concentration in surface seawaters was still not high enough, although elevated to some extent (Fig. 3) compared to deeper times backward, to enable large metazoans but only small-sized taxa to sustain their life. In addition, the frequent invasions of deep anoxic waters onto the shallow-water oxygenated areas could have restricted the expansion of shallow-water ecological niches (Li et al., 2010), hindering ecological exploitation and innovation for metazoans. These stressful factors may account for the origination and diversification of only small shelly fauna rather than of large forms from the onset of Cambrian through Tommotian (Knoll and Carroll, 1999; Zhu et al., 2003; Marshall, 2006).

However, it seems that the enhanced skeletonization of many metazoans from the Cambrian was not simply a response of elevated oxygen concentration in oceans (e.g., Raff and Raff, 1970) in view of differential skeletal biomineralization in different taxa, for example, siliceous skeletons for sponges, and calcite skeletons for echinoderms and trilobites. Other factors such as vast changes in oceanic chemistry, i.e., boost in silica concentration (Fig. 3; Chen et al., 2009; Wang et al., 2012) and rapid increase in seawater [Ca^{2+}] concentration (Brennan et al., 2004, Stanley, 2006; Zhuravlev and Wood, 2008), could have provided additional ecological opportunities for some taxa to make themselves adapt and thereby promote further developmental innovation, enabling to secrete exoskeletons compositionally to fit the ambient waters (Skimiss, 1989; Stanley, 2006), and ultimately resulting in differential biomineralization of some skeletonized taxa.

6. Conclusions

This study presents the expanded new C–S isotopic data and Fe speciation across the deep-water E–C successions at Longbizui, western Hunan in South China. The recognition of a large negative C_{org} isotopic excursion, together with the stratigraphic marker bed, enables to place the E–C boundary in the middle of Liuchapo Formation. Two major phases (I and II) are identified in the deep ocean evolution of E–C transition. Phase I is characterized by high Fe_{HR}/Fe_T (>0.38) and low Fe_P/Fe_{HR} ratios (<0.80) and roughly coupled C–S cycling, indicating an anoxic, ferruginous-dominated deep ocean. Phase II is characterized by rapid decreases in $\delta^{34}S_{py}$ values and Fe_{HR}/Fe_T ratios (mostly <0.38), and decoupled C–S cycling, indicating an oxic deep ocean. Transition from an anoxic to the oxic deep ocean coincided with the sudden appearance of large-body sponge fauna, which was temporally linked to the Chengjiang Biota in the middle Early Cambrian (Atdabanian) on Yangtze platform. Boost in oxygen concentration in the ocean, possibly together with other factors, could have triggered and accelerated the explosive bioradiation of skeletonized animals in the Early Cambrian.

Acknowledgments

This work was supported by the National Natural Science Foundation of China (project 40839907) and National Key Basic Research Project (2005CB422101). We thank Fusong Zhang and Liangjun Feng for their assistance in lab work. Insightful comments from A.J. Christie-Blick and an anonymous reviewer, and Chief Editor U. Brand are highly acknowledged.

References

Amthor, J.E., Grotzinger, J.P., Schröder, S., Bowring, S.A., Ramezani, J., Martin, M.W., Matter, A., 2003. Extinction of *Cloudina* and *Namacalathus* at the Precambrian–Cambrian boundary in Oman. Geology 31, 431–434.

Babcock, L.E., Zhang, W., Leslie, S.A., 2001. The Chenjiang Biota: record of the Early Cambrian diversification of life and clues to exceptional preservation of fossils. GSA Today 11, 4–9.

Bartley, J.K., Kah, L.C., 2004. Marine carbon reservoir, C_{org}–C_{carb} coupling, and the evolution of the Proterozoic carbon cycle. Geology 32, 129–132.

Behrenfeld, M.J., Bale, A.J., Kolber, A.S., Aiken, J., Falkowski, P.G., 1996. Confirmation of iron limitation of phytoplankton photosynthesis in the equatorial Pacific Ocean. Nature 383, 508–511.

Berner, R.A., 1989. Biogeochemical cycles of carbon and sulfur and their effect on atmospheric oxygen over Phanerozoic time. Global and Planetary Change 1, 97–122.

Berner, R.A., Petsch, S.T., 1998. The sulfur cycle and atmospheric oxygen. Science 282, 1426–1427.

Bottomley, D.J., Veizer, J., Nielsen, H., Moczydlowska, M., 1992. Isotopic composition of disseminated sulfur in Precambrian sedimentary rocks. Geochimica et Cosmochimica Acta 56, 3311–3322.

Brasier, M.D., Corfield, R.M., Derry, L.A., Rozanov, A.Y., Zhuravlev, A.Y., 1994. Multiple $\delta^{13}C$ excursions spanning the Cambrian explosion to the Botomian crisis in Siberia. Geology 22, 455–458.

Brasier, M.D., Shields, G., Kuleshov, V.N., Zhegallo, E.A., 1996. Integrated chemo- and biostratigraphic calibration of early animal evolution: Neoproterozoic-Early Cambrian of southwest Mongolia. Geological Magazine 133, 445–485.

Brennan, S.T., Lowenstein, T.K., Horita, J., 2004. Seawater chemistry and the advent of biocalcification. Geology 32, 473–476.

Butterfield, N.J., 2007. Macroevolution and macroecology through deep time. Palaeontology 50, 41–55.

Canfield, D.E., 2004. The evolution of the Earth surface sulfur reservoir. American Journal of Science 304, 839–861.

Canfield, D.E., Teske, A., 1996. Late Proterozoic rise in atmospheric oxygen concentration inferred from phylogenetic and sulphur-isotope studies. Nature 382, 127–132.

Canfield, D.E., Raiswell, R., Westrich, J.T., Reaves, C.M., Berner, R.A., 1986. The use of chromium reduction in the analysis of reduced inorganic sulfur in sediments and shales. Chemical Geology 54, 149–155.

Canfield, D.E., Poulton, S.W., Narbonne, G.M., 2007. Late Neoproterozoic deep-ocean oxygenation and the rise of animal life. Science 315, 92–95.

Canfield, D.E., Poulton, S.W., Knoll, A.H., Narbonne, G.M., Ross, G., Goldberg, T., Strauss, H., 2008. Ferruginous conditions dominated later Neoproterozoic deep-water chemistry. Science 321, 949–952.

Chang, H.J., Chu, X.L., Feng, L.J., Huang, J., 2009. Terminal Ediacaran axoxia in deep-ocean: Trace element evidence from cherts of the Liuchapo Formation, South China. Science China (Series D). Earth Science 52, 807–822.

Charlou, J.L., Donval, J.P., Fouquet, Y., Jean-Baptiste, P., Holm, N., 2002. Geochemistry of high H_2 and CH_4 vent fluids issuing from ultramafic rocks at the rainbow hydrothermal filed (36°14′N, MAR). Chemical Geology 191, 345–359.

Chen, D.Z., Wang, J.G., Qing, H.R., Yan, D.T., Li, R.W., 2009. Hydrothermal venting activities in the Early Cambrian, South China: petrological, geochronological and stable isotopic constrains. Chemical Geology 258, 168–181.

Condon, D., Zhu, M., Bowring, S., Wang, W., Yang, A., Jin, Y., 2005. U–Pb ages from the Neoproterozoic Doushantuo Formation, China. Science 308, 95–98.

Cooper, D.J., Watson, A.J., Nightingale, P.D., 1996. Large decrease in ocean-surface CO_2 fugacity in response to in situ iron fertilization. Nature 383, 511–513.

Corsetti, F.A., Hagadorn, J.M., 2000. Precambrian–Cambrian transition: Death Valley, United States. Geology 28, 299–302.

Dean, W.E., Arthur, M.A., Claypool, G.E., 1986. Depletion of ^{13}C in Cretaceous marine organic matter: source, diagenetic, or environmental signals? Marine Geology 70, 119–157.

Erwin, D.H., Laflamme, M., Tweedt, S.M., Sperling, E.A., Pisani, D., Peterson, K.J., 2011. The Cambrian conundrum: early divergence and later ecological success in the early history of animals. Science 334, 1091–1097.

Falkowski, P.G., Barber, R.T., Smetacek, V., 1998. Biogeochemical controls and feedback on ocean primary production. Science 281, 200–206.

Fike, D.A., Grotzinger, J.P., Pratt, L.M., Summons, R.E., 2006. Oxidation of the Ediacaran Ocean. Nature 444, 744–747.

Freeman, K.H., Hayes, 1992. Fractionation of carbon isotopes by phytoplankton and estimates of ancient CO_2 levels. Global Biogeochemical Cycles 6, 185–198.

Gill, B.C., Lyons, T.W., Saltzman, M.R., 2007. Parallel, high-resolution carbon and sulfur isotope records of the evolving Paleozoic marine sulfur reservoir. Palaeogeography, Palaeoclimatology, Palaeoecology 256, 156–173.

Gill, B.C., Lyons, T.W., Young, S.A., Kump, L.R., Knoll, A.H., Saltzman, M.R., 2011. Geochemical evidence for widespread euxinia in the Later Cambrian Ocean. Nature 469, 80–83.

Goldberg, T., Poulton, S.W., Strauss, H., 2005. Sulfur and oxygen isotope signatures of late Neoproterozoic to early Cambrian sulphates, Yangtze Platform, China: diagenetic constraints and seawater evolution. Precambrian Research 137, 223–241.

Goldberg, T., Strauss, H., Guo, Q., Liu, C., 2007. Reconstructing marine redox conditions for the early Cambrian Yangtze Platform: evidence from biogenic sulphur and organic carbon isotopes. Palaeogeography, Palaeoclimatology, Palaeoecology 254, 174–193.

Graham, J.B., Dudley, R., Aguilar, N.M., Gans, C., 1995. Implications of the late Palaeozoic oxygen pulse for physiology and evolution. Nature 375, 117–120.

Guo, Q., Strauss, H., Liu, C., Goldberg, T., Zhu, M., Pi, D., Heubeck, C., Vernhet, E., Yang, X., Fu, P., 2007. Carbon isotopic evolution of the terminal Neoproterozoic and early Cambrian: evidence from the Yangtze Platform, South China. Palaeogeography, Palaeoclimatology, Palaeoecology 254, 140–157.

Habicht, K.S., Gade, M., Thamdrup, B., Berg, P., Canfield, D.E., 2002. Calibration of sulfate levels in the Archean ocean. Science 298, 2372–2374.

Halverson, G.P., Hurtgen, M.T., 2007. Ediacaran growth of the marine sulfate reservoir. Earth and Planetary Science Letters 263, 32–44.

Hayes, J.M., Strauss, H., Kaufman, A.J., 1999. The abundance of ^{13}C in marine organic matter and isotopic fractionation in the global biogeochemical cycle of carbon during the past 800 Ma. Chemical Geology 161, 103–125.

He, S., Yu, G., 1992. The small shelly fossils from the Palaeocambrian Meishucunian stage in western Zhejiang. Zhejiang Geology 8, 1–7.

Herzig, P.M., Hannington, M.D., Arribas Jr., A., 1998. Sulfur isotopic composition of hydrothermal precipitates from the Lau back-arc: implications for magmatic contributions to seafloor systems. Mineralium Deposita 33, 226–237.

Holland, H.D., 2006. The oxygenation of the atmosphere and oceans. Philosophical Transactions of the Royal Society of London, Series B 361, 903–915.

Hou, X.G., Aldridge, R.J., Bergstrom, J., Sieveter, D.J., Feng, X., 2004. The Cambrian Fossils of Chengjiang, China: The Flowering of Early Animal Life. Blackwell Publ, Oxford. 233 pp.

Hurtgen, M.T., Arthur, M.A., Halverson, G.P., 2005. Neoproterozoic sulfur isotopes, the evolution of microbial sulfur species, and the burial efficiency of sulfide as sedimentary sulfide. Geology 33, 41–44.

Hurtgen, M.T., Pruss, S.T., Knoll, A.H., 2009. Evaluating the relationship between the carbon and sulfur cycles in the later Cambrian ocean: an example from the Port au Port Group, western Newfoundland, Canada. Earth and Planetary Science Letters 281, 288–297.

Ishikawa, T., Ueno, Y., Komiya, T., Sawaki, Y., Han, J., Shu, D., Li, Y., Maruyama, S., Yoshida, N., 2008. Carbon isotope chemostratigraphy of a Precambrian/Cambrian boundary section in the Three Gorge area, South China: prominent global-scale isotope excursions just before the Cambrian Explosion. Gondwana Research 14, 193–208.

Jiang, G., Kennedy, M.J., Christie-Blick, N., Wu, H., Zhang, S., 2006. Stratigraphy, sedimentary structures, and textures of the late Neoproterozoic Doushantuo cap carbonate in South China. Journal of Sedimentary Research 76, 978–995.

Jiang, G., Kaufman, A.J., Christie-Blick, N., Zhang, S., Wu, H., 2007a. Carbon isotope variability across the Ediacaran Yangtze platform in South China: implication for a large surface-to-deep ocean $\delta^{13}C$ gradient. Earth and Planetary Science Letters 261, 303–320.

Jiang, S., Yang, J., Ling, H., Chen, Y., Feng, H., Zhao, K., Ni, P., 2007b. Extreme enrichment of polymetallic Ni–Mo–PGE–Au in lower Cambrian black shales of South China: an Os isotope and PGE geochemical investigation. Palaeogeography, Palaeoclimatology, Palaeoecology 254, 217–228.

Jiang, S., Pi, D., Heubeck, C., Frimmel, H., Liu, Y., Deng, H., Ling, H., Yang, H., 2009. Early Cambrian ocean anoxia in South China. Nature 459, E5–E6.

Jiang, G., Wang, X., Shi, X., Zhang, S., Xiao, S., Dong, J., 2010. Organic carbon isotope constraints on the dissolved organic carbon (DOC) reservoir at the Cryogenian–Ediacaran transition. Earth and Planetary Science Letters 299, 159–168.

Johnston, D.T., Poulton, S.M., Dehler, C., Porter, S., Husson, J., Canfield, D.E., Knoll, A.H., 2010. An emerging picture of Neoproterozoic ocean chemistry: insights from the Chuar Group, Grand Canyon, USA. Earth and Planetary Science Letters 290, 64–73.

Kaufman, A.J., Knoll, A.H., 1995. Neoproterozoic variations in the C-isotopic composition of seawater: stratigraphic and biogeochemical implications. Precambrian Research 73, 27–49.

Kaufman, A.J., Knoll, A.H., Semikhatov, M.A., Grotzinger, J.P., Jacobsen, S.B., Adams, W., 1996. Integrated chronostratigraphy of Proterozoic–Cambrian boundary beds in the western Anabar region, northern Siberia. Geological Magazine 133, 509–533.

Kimura, H., Watanabe, Y., 2001. Oceanic anoxia at the Precambrian–Cambrian boundary. Geology 29, 995–998.

Kimura, H., Matsumoto, R., Kakuwa, Y., Hamdi, B., Zibaseresht, H., 1997. The Vendian-Cambrian $\delta^{13}C$ record, North Iran: evidence for overturning of the ocean before the Cambrian Explosion. Earth and Planetary Science Letters 147, E1–E7.

Knoll, A.H., Walter, M.R., 1992. Latest Proterozoic stratigraphy and Earth history. Nature 356, 673–678.

Knoll, A.H., Carroll, S.B., 1999. Early animal evolution: emerging views from comparative biology and geology. Science 284, 2129–2137.

Kolber, Z.S., Barber, R.T., Coale, K.H., Fitzwater, S.E., Greene, R.M., Johnson, K.S., Lindley, S., Falkowski, P.G., 1994. Iron limitation of phytoplankton photosynthesis in the equatorial Pacific Ocean. Nature 374, 145–148.

Kump, L.R., Arthur, M.A., 1999. Interpreting carbon-isotope excursions: carbonates and organic matter. Chemical Geology 161, 181–198.

Kump, L.R., Arthur, M.A., Patzkowsky, M.E., Gibbs, M.T., Pinkus, D.S., Sheehan, P.M., 1999. A weathering hypothesis for glaciation at high atmospheric pCO_2 during the Late Ordovician. Palaeogeography, Palaeoclimatology, Palaeoecology 152, 173–187.

Lambert, I.B., Walter, M.R., Zang, W., Lu, S., Ma, G., 1987. Palaeoenvironment and carbon isotope stratigraphy of Upper Proterozoic carbonates of the Yangtze Platform. Nature 328, 140–142.

Li, C., He, J., Ye, H., 1990. Discovery of Early Cambrian trilobites in Guichi of Anhui Province. Journal of Stratigraphy 14, 159–160 (in Chinese with English abstract).

Li, C.-W., Chen, J.Y., Hua, T.E., 1998. Precambrian sponges with cellular structure. Science 279, 879–882.

Li, C., Love, G.D., Lyons, T.W., Fike, D.A., Sessions, A.L., Chu, X., 2010. A stratified redox model for the Ediacaran ocean. Science 328, 80–83.

Logan, G.A., Hayes, J.M., Hieshima, G.B., Summons, R.E., 1995. Terminal Proterozoic reorganization of biogeochemical cycles. Nature 376, 53–56.

Maloof, A.C., Ramezani, J., Bowring, S.A., Fike, D.A., Porter, S.M., Mazouad, M., 2010. Constraints on early Cambrian carbon cycling from the duration of the Nemakit–Daldynian–Tommotian boundary $\delta^{13}C$ shift, Morocco. Geology 38, 623–626.

Marshall, C.R., 2006. Explaining the Cambrian "Explosion" of animals. Annual Review of Earth and Planetary Science 34, 355–384.

McFadden, K.A., Huang, J., Chu, X., Jiang, G., Kaufman, A.J., Zhou, C., Yuan, X., Xiao, S., 2008. Pulsed oxidation and biological evolution in the Ediacaran Doushantuo Formation. Proceedings of the National Academy of Sciences 105, 3197–3202.

Nursall, J.R., 1959. Oxygen as a prerequisite to the origin of the metazoan. Nature 183, 1170–1172.

Payne, J.L., Boyer, A.G., Brown, J.H., Finnegan, S., Kowalewski, M., Krause Jr., R.A., Lyons, S.K., McClain, C.R., McShea, D.W., Novack-Gottshall, P.M., Smith, F.A., Stempien, J.A., Wang, S.C., 2009. Two-phase increase in the maximum size of life over 3.5 billion - years reflects biological innovation and environmental opportunity. Proceedings of the National Academy of Sciences 106, 24–27.

Popp, B.N., Takigiku, R., Hayes, J.M., Louda, J.W., Baker, E.W., 1989. The post-Paleozoic chronology and mechanism of ^{13}C depletion in primary marine organic matter. American Journal of Science 289, 436–454.

Poulton, S.W., Canfield, D.E., 2005. Development of a sequential extraction procedure for iron: implications for iron partitioning in continentally derived particulates. Chemical Geology 214, 209–221.

Poulton, S.W., Canfield, D.E., 2011. Ferruginous conditions: a dominant feature of the ocean through Earth's history. Elements 7, 107–112.

Poulton, S.W., Fralick, P.W., Canfield, D.E., 2004. The transition to a sulphidic ocean 1.84 billion years ago. Nature 431, 173–177.

Poulton, S.W., Fralick, P.W., Canfield, E., 2010. Spatial variability in oceanic redox structure 1.8 billion years ago. Nature Geoscience 3, 486–490.

Qian, Y., Yin, G., 1984. Small shelly fossils from the lowest Cambrian in Guizhou. Professional Papers of Stratigraphy and Palaeontology 13, 91–124 (in Chinese).

Raff, R.A., Raff, E.C., 1970. Respiratory mechanisms and metazoan fossil record. Nature 228, 1003–1005.

Raiswell, R., Canfield, D.E., 1998. Sources of iron for pyrite formation in marine sediments. American Journal of Science 298, 219–245.

Ries, J.B., Fike, D.A., Pratt, L.M., Lyons, T.W., Grotzinger, J.P., 2009. Superheavy pyrite ($\delta^{34}S_{pyr} > \delta^{34}S_{CAS}$) in the terminal Proterozoic Nama Group, southern Namibia: a

consequence of low seawater sulfate at the dawn of animal life. Geology 37, 743–746.
Sælen, G., Raiswell, R., Talbot, M.R., Skei, J.M., Bottrell, B., 1993. Heavy sedimentary sulfur isotopes as indicators of super-anoxic bottom-water conditions. Geology 21, 1091–1094.
Shen, Y., Schidlowski, M., 2000. New C isotope stratigraphy from southwest China: implications for the placement of the Precambrian–Cambrian boundary on the Yangtze Platform and Global correlations. Geology 28, 623–626.
Shen, Y., Zhao, R., Chu, X., Lei, J., 1998. The carbon and sulfate isotope signature in the Precambrian–Cambrian transition series of the Yangtze Platform. Precambrian Research 89, 77–86.
Shen, Y., Zhang, T., Hoffman, P., 2008. On the coevolution of Ediacran oceans and animals. Proceedings of the National Academy of Sciences 152, 7376–7381.
Skimiss, K., 1989. Biomineralization in the context of geological time. Royal Society of Edinburgh Earth Science 80, 193–199.
Stanley, S.M., 2006. Influence of seawater chemistry on biomineralization throughout Phanerozoic time; Paleontological and experimental evidence. Palaeogeography, Palaeoclimatology, Palaeoecology 232, 214–236.
Steiner, M., Wallis, E., Erdtmann, B.-D., Zhao, Y.L., Yang, R.D., 2001. Submarin-hydrothermal exhalative ore layers in black shales from South China and associated fossils—insights into a Lower Cambrian facies and bio-evolution. Palaeogeography, Palaeoclimatology, Palaeoecology 169, 165–191.
Steiner, M., Zhu, M., Zhao, Y., Erdtmann, B.-D., 2005. Lower Cambrian Burgess Shale-type fossil associations of South China. Palaeogeography, Palaeoclimatology, Palaeoecology 220, 129–152.
Steiner, M., Li, G.X., Qian, Y., Zhu, M.Y., Erdtmann, B.-D., 2007. Neoproterozoic to early Cambrian small shelly fossil assemblages and revised biostratigraphic correlation of the Yangtze Platform (China). Palaeogeography, Palaeoclimatology, Palaeoecology 254, 67–99.
Strauss, H., 1997. The isotopic composition of sedimentary sulfur through time. Palaeogeography, Palaeoclimatology, Palaeoecology 132, 97–118.
Strauss, H., Des Marais, D.J., Hayes, J.M., Summons, R.E., 1992. The carbon-isotopic record. In: Schopf, J.W., Klein, C. (Eds.), The Proterozoic Biosphere: A Multidisciplinary Study: Cambrian. Cambridge University Press, UK, pp. 117–127.
Wang, J., Li, Z.-X., 2003. History of Neoproterozoic rift basins in South China: implications for Rodinia break-up. Precambrian Research 122, 141–158.
Wang, J.G., Chen, D.Z., Wang, D., Yan, D.T., Zhou, X.Q., Wang, Q.C., 2012. Petrology and geochemistry of chert on the marginal zone of Yangtze Platform, western Hunan, South China during the Ediacaran–Cambrian transition. Sedimentology 59, 809–829.
Wille, M., Nägler, T.F., Lehmann, B., Schröder, S., Kramers, J.D., 2009. Hydrogen sulphide release to surface waters at the Precambrian/Cambrian boundary. Nature 453, 767–769.
Xiao, S., Hu, J., Yuan, X., Parsley, R.L., Cao, R., 2005. Articulated sponges from the Lower Cambrian Hetag Formation in southern AnHui, South China: their age and implications for the early evolution of sponges. Palaeogeography, Palaeoclimatology, Palaeoecology 220, 89–117.
Yan, D.T., Chen, D.Z., Wang, Q.C., Wang, J.G., 2012. Predominance of stratified anoxic Yangtze Sea interrupted by short-term oxygenation during the Ordo–Silurian transition. Chemical Geology 291, 69–78.
Yang, A., Zhu, M., Zhang, J., Li, G., 2003. Early Cambrian eodiscoid trilobites of the Yangtze Platform and their stratigraphic implication. Progress in Natural Science 13, 861–866.
Yuan, X., Xiao, S., Parsley, R.L., Zhou, C., Chen, Z., Hu, J., 2002. Towering sponges in an Early Cambrian Lagerstätte: disparity between nonbilaterian and bilaterian epifaunal tierers at the Neoproterozoic–Cambrian transition. Geology 30, 363–366.
Zhang, X.-G., Pratt, B.R., 1994. New and extraordinary Early Cambrian sponge spicule assemblage from China. Geology 22, 43–46.
Zhang, Y., Jiang, G., Zhang, J., Song, B., Kennedy, M.J., Christie-Blick, N., 2005. U–Pb sensitive high-resolution ion microprobe ages from the Doushantuo Formation in south China: constraints on late Neoproterozoic glaciations. Geology 33, 473–476.
Zhao, X., Li, G.X., 2006. Early Cambrian sponge spicule fossils from Zhenba County, southern Shaanxi Province. Acta Micropalaeontologica Sinica 23, 281–294 (in Chinese with English abstract).
Zhou, C., Zhang, J., Li, G., Yu, Z., 1997. Carbon and oxygen isotopic record of the Early Cambrian from the Xiaotan section, Yunnan, South China. Scientia Geologica Sinica 32, 201–211 (in Chinese with English abstract).
Zhu, M., Zhang, J., Steiner, M., Yang, A., Li, G., Erdtman, B.D., 2003. Sinian-Cambrian stratigraphic framework for shallow- to deep-water environments of the Yangtze Platform: an integrated approach. Progress in Natural Science 13, 951–960.
Zhuravlev, A.Y., Wood, R., 2008. Eve of biomineralization: controls on skeletal mineralogy. Geology 36, 923–926.